

Towards a predictive model of Ca^{2+} puffs

R Thul,¹ K Thurley,² and M Falcke²

¹*School of Mathematical Sciences, University of Nottingham, Nottingham, NG7 2RD, UK*

²*Mathematical Cell Physiology, Max Delbrück Centre for Molecular Medicine,
Robert Rössle Str. 10, 13092 Berlin, Germany*

(Dated: July 29, 2009)

Abstract

We investigate key characteristics of Ca^{2+} puffs in deterministic and stochastic frameworks that all incorporate the cellular morphology of IP_3 receptor channel clusters. In a first step, we numerically study Ca^{2+} liberation in a three dimensional representation of a cluster environment with reaction-diffusion dynamics in both the cytosol and the lumen. These simulations reveal that Ca^{2+} concentrations at a releasing cluster range from $80 \mu\text{M}$ to $170 \mu\text{M}$ and equilibrate almost instantaneously on the time scale of the release duration. These highly elevated Ca^{2+} concentrations eliminate Ca^{2+} oscillations in a deterministic model of an IP_3R channel cluster at physiological parameter values as revealed by a linear stability analysis. The reason lies in the saturation of all feedback processes in the IP_3R gating dynamics, so that only fluctuations can restore experimentally observed Ca^{2+} oscillations. In this spirit, we derive master equations that allow us to analytically quantify the onset of Ca^{2+} puffs and hence the stochastic time scale of intracellular Ca^{2+} dynamics. Moving up the spatial scale, we suggest to formulate cellular dynamics in terms of waiting time distribution functions. This approach prevents the state space explosion that is typical for the description of cellular dynamics based on channel states and still contains information on molecular fluctuations. We illustrate this method by studying global Ca^{2+} oscillations.

The initiation of Ca^{2+} puffs marks the first step of vital Ca^{2+} signals observed in a multitude of cells ranging from localised elevations of the cytosolic Ca^{2+} concentration over abortive waves to whole cell patterns. The very nature of Ca^{2+} puffs as Ca^{2+} liberation through a cluster of ion channels demands a close investigation of the relationships between properties of a Ca^{2+} puff and the micro environment of a cluster. Here, we demonstrate that the spatial confinement of channel clusters leads to Ca^{2+} concentrations around a conducting cluster that are 2–3 orders of magnitude larger than bulk concentrations. These give rise to steep gradients around a cluster and highlight that cells do not resemble well-stirred reactors with spatially homogenous concentration profiles. Coupling such large Ca^{2+} concentrations to deterministic gating dynamics of an ion channel cluster reveals that fluctuations drive experimentally observed Ca^{2+} oscillations. Consequently, we derive a probabilistic description of a cluster that allows us to quantitatively predict the random time scale of Ca^{2+} puff initiation. We then derive cellular dynamics from puff characteristics.

I. INTRODUCTION

A paramount task of all cells is to maintain reliable and precise signalling. Such signalling events often consist of cascades of interactions, where the output of one step serves as input to the succeeding one. Importantly, various components in such signalling pathways may be positioned at different cellular locations. An example is the synthesis of cyclic adenosine monophosphate (cAMP), one of the most important second messengers [1]. When hormones in the extracellular space stimulate G-protein coupled receptors that are located in the plasma membrane, membrane bound adenylyl cyclases are activated. In turn, they catalyse the formation of cAMP from adenosine triphosphate (ATP), which diffuses through the cytosol. cAMP then triggers a multitude of reactions including gene expression. Hence, the overall signal may travel from the extracellular space through interactions in the plasma membrane and the cytosol to the nucleus. This layout immediately reveals that the concentration of the signalling molecules involved varies considerably in space and time. The concentration of activated adenylyl cyclase is only high in regions of activated G-protein coupled receptors. Consequently, cAMP is only synthesised in the same region giving rise

to huge concentration gradients around it [2]. They persist only as long as the stimulus is present and therefore vary in time.

The cAMP pathway illustrates spatio-temporal characteristics that are equally applicable to another major second messenger: Calcium. Intracellular Calcium plays an important role in fertilisation, secretion of enzymes, muscle contraction, neuronal computing or programmed cell death, to name only a few [3, 4]. Among the different routes that lead to an increase in cytosolic Calcium, one shares similarities with the synthesis of cAMP. Upon stimulation of G-protein coupled receptors, inositol 1,4,5-trisphosphate (IP₃) is formed at the plasma membrane, which then diffuses through the cytosol to receptors that are located on the membrane of the endoplasmic reticulum (ER). Upon binding to these IP₃ receptors (IP₃Rs), Ca²⁺ is liberated from the ER resulting in a transient increase of the cytosolic Ca²⁺ concentration. Similar to the localised production of IP₃ at the plasma membrane, release of Ca²⁺ from the ER occurs only at specific sites, which correspond to clusters of IP₃R channels. Depending on the cell type, these clusters form either regular or irregular arrays. For instance, in *Xenopus* oocytes, clusters are scattered randomly on the membrane of the ER with distances between 2–7 μm [5]. To appreciate that such a separation is indeed responsible for localised elevations of the intracellular Ca²⁺ concentration, we need to consider two points. Firstly, the open probability of IP₃R channels depends on the cytosolic Ca²⁺ concentration. At base level, IP₃Rs are unlikely to be activated, but a small increase in the Ca²⁺ concentration leads to a significant increase in the open probability [6]. Therefore, Ca²⁺ that is released from a cluster and diffuses to adjacent clusters amplifies the open probability there. However, this increase is minute since, secondly, the diffusion length of Ca²⁺ in the cytosol is approximately 1 μm , so that only little of the liberated Ca²⁺ from one cluster reaches the neighbouring clusters. Considering Ca²⁺ diffusion as the main coupling mechanism between nearby clusters, the coupling is weak, which in turn gives rise to spatially localised Ca²⁺ release.

This picture is even emphasised by the small lateral extension of a cluster. Latest results demonstrate that clusters consist of only 4–8 tightly packed channels, which restricts the diameter of a cluster to less than 100 nm [7]. These new findings contrast earlier values of 100–300 nm, which were based on theoretical estimates of 5–40 channels per cluster [8, 9]. Such low copy numbers of channel molecules allow us to characterise the state of a cluster in terms of channel states. Taking into account that these channel states depend on constant

binding and unbinding of Ca^{2+} and IP_3 at designated binding sites, the stochastic nature of chemical association and dissociation entails that channels switch randomly between different states. These fluctuations readily lead to stochastic cluster states since the number of channels per cluster is too small to average over channel state fluctuations. Hence, a cluster of IP_3R channels presents a spatially localised release site whose intrinsic dynamics is highly stochastic.

From a modeller's perspective, these ideas impose strong bounds on the methods to analyse intracellular Ca^{2+} dynamics. The traditional route was based on the assumption that cells correspond to well-stirred reactors, i.e. all dynamics was deterministic and spatially homogenous. Early studies in this spirit [10–14] yielded valuable insights and paved the way for more sophisticated experimental and theoretical investigations. Even today, such classical approaches may generate new predictions and hence serve as a starting point for a more elaborate analysis. However, in the quest to unravel the full dynamical repertoire of intracellular Ca^{2+} dynamics, we need to proceed along new avenues of spatially resolved models that treat Ca^{2+} release as a stochastic variable. This corresponds to a transition from deterministic ordinary differential equations to partial differential equations coupled to stochastic schemes that describe the dynamics of IP_3R channels. In this article, we review quantitative results for release currents through a cluster of IP_3R channels that underpin the notion of huge gradients around a conducting cluster. After demonstrating that these gradients are responsible to eliminate Ca^{2+} oscillations in deterministic models of Ca^{2+} release, we report on stochastic schemes to quantitatively model single cluster dynamics. Finally, we suggest a non-Markovian formulation of intracellular Ca^{2+} dynamics circumventing the drawbacks of partial differential equations and state space explosion at the cell level.

II. RELEASE CURRENTS THROUGH A CLUSTER OF IP_3R CHANNELS

Calcium released through clusters of IP_3R channels does not only induce a multitude of downstream signals, but it feeds immediately back on the dynamics of IP_3 receptors. Although the precise mechanistic details are still actively debated (see [15–17] for recent reviews), the role of Calcium as both an agonist and antagonist of the IP_3 receptor is well established. Since such feed-backs depend on binding and unbinding of Ca^{2+} to specific sites on the receptor, estimates of the local Ca^{2+} concentration at a liberating cluster are an

essential ingredient of any modelling work. However, the diameter of IP₃R channel clusters ranges between 20-300 nm, which does not allow for any measurement. Hence, we performed numerical simulations to gain a quantitative insight into Ca²⁺ release. Figure 1 depicts the geometry that we have chosen. The set-up mimics the immediate environment of an IP₃R

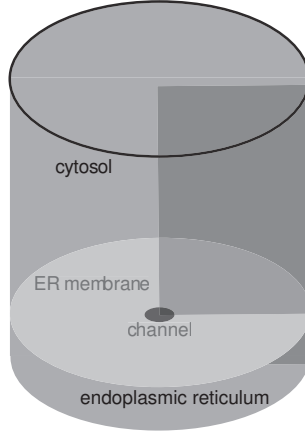


FIG. 1: Geometrical setup for release simulations. The liberating cluster is presented by a concentric hole in the the ER membrane.

cluster. On this scale, the membrane of the ER can be considered locally flat and adjacent clusters are sufficiently apart. Hence, there is only one cluster in the cylindrical simulation volume, in which the lower part corresponds to the ER and the upper part to the cytosol. The membrane between the two compartments is located at constant height, and the IP₃R cluster is presented by a hole in the centre of the membrane. For the time being, we do not model any gating activity, but consider the situation when a fixed number of channels is already open. This translates into a Ca²⁺ flux through a conducting area of constant radius R . The time evolution of the Ca²⁺ concentration in the cytosol is governed by the reaction-diffusion equations

$$\frac{\partial c}{\partial t} = D\nabla^2 c - k_m^+(B_m - b_m)c + k_m^- b_m - k_s^+(B_s - b_s)c + k_s^- b_s, \quad (1a)$$

$$\frac{\partial b_m}{\partial t} = D_m \nabla^2 b_m + k_m^+(B_m - b_m)c - k_m^- b_m, \quad (1b)$$

$$\frac{\partial b_s}{\partial t} = k_s^+(B_s - b_s)c - k_s^- b_s. \quad (1c)$$

Here, c denotes the concentration of free cytosolic Calcium, b_m and b_s refer to the concentrations of cytosolic Ca²⁺ bound mobile and cytosolic Ca²⁺ bound stationary buffer,

respectively. The first term of the right hand side in equation (1a) represents diffusion, whereas the remaining expressions correspond to unbinding from and binding to mobile and stationary buffers, respectively. Note that both buffer types obey the same kinetic scheme, but only the mobile buffer diffuses. The dynamics in the ER takes the same form as in the cytosol, i.e.

$$\frac{\partial E}{\partial t} = D_E \nabla^2 E - k_{\text{Em}}^+ (B_{\text{Em}} - b_{\text{Em}}) E + k_{\text{Em}}^- b_{\text{Em}} - k_{\text{Es}}^+ (B_{\text{Es}} - b_{\text{Es}}) E + k_{\text{Es}}^- b_{\text{Es}}, \quad (2a)$$

$$\frac{\partial b_{\text{Em}}}{\partial t} = D_{\text{Em}} \nabla^2 b_{\text{Em}} + k_{\text{Em}}^+ (B_{\text{Em}} - b_{\text{Em}}) E - k_{\text{Em}}^- b_{\text{Em}}, \quad (2b)$$

$$\frac{\partial b_{\text{Es}}}{\partial t} = k_{\text{Es}}^+ (B_{\text{Es}} - b_{\text{Es}}) E - k_{\text{Es}}^- b_{\text{Es}}, \quad (2c)$$

where E corresponds to the free luminal Ca^{2+} concentration, and b_{Em} and b_{Es} denote the concentration of luminal Ca^{2+} bound mobile and luminal Ca^{2+} bound stationary buffer, respectively. The two compartments are coupled by fluxes through the ER membrane. Ca^{2+} flows through the conducting cluster according to

$$J = \Psi \frac{E - \alpha c}{\beta + \gamma E + \delta c}, \quad r \leq R. \quad (3)$$

Equation (3) corresponds to a saturating barrier model of a conducting pore with a single ion binding site [18], which was suggested in measurements by Bezprozvanny and Ehrlich [19]. The five constants Ψ , α , β , γ , δ were determined by fitting flux simulations to experimental data from [19] as outlined in [20]. Outside the cluster, a constant leak occurs that is proportional to the concentration difference over the membrane. In addition, Ca^{2+} is pumped back from the cytosol into the ER by sarco-endoplasmic reticulum Ca^{2+} ATPase (SERCA) pumps, which we model by a Hill function with coefficient 2:

$$J = P_l (E - c) - P_p \frac{c^2}{K_d^2 + c^2}, \quad r > R \quad (4)$$

Under the assumption that Fick's law holds, these fluxes relate to the concentration fields by

$$D \frac{\partial c}{\partial z} = D_E \frac{\partial E}{\partial z} = -J. \quad (5)$$

No-flux boundary conditions were imposed at the surfaces of the cylinder. We employed an explicit scheme to discretise the diffusion operator and a 4th order Runge-Kutta algorithm for the reaction terms [21]. Spatial discretisation was 2 nm for single channel simulations, $2\sqrt{2}$ nm and 4 nm for larger clusters.

In a first step, we will apply our framework to Ca^{2+} liberation through a single IP_3R channel. This requires us to determine the radius R of the conducting membrane patch, i.e. the size of a channel pore. Direct data for IP_3R channels is still unavailable, but Jiang et al. recently measured the three-dimensional structure of an IP_3R channel by cryo-electron microscopy of purified receptors. Their data suggest an overall extension of approximately 15 nm [22]. This is comparable to results by Suhara et al. [23] who investigated IP_3R channels in a fluid environment employing atomic force microscopy. Both studies agree with estimates for RyR channels, which represent another major Ca^{2+} releasing channel [24]. Mejia-Alvarez et al. argue that the pore size can be well approximated by the extension of the luminal sponge, i.e. the volume around the pore in which negative charges reside [25]. They conclude that the pore measures between 5–10 nm. Based on these findings, we set the single channel radius R_S to 6 nm. The left panel in Figure 2 shows the concentration profile around a single channel at two different time points after release began. The peak concentration of almost $80 \mu\text{M}$ is obtained within the first microsecond. After that, the profile broadens slightly, but the overall shape remains almost constant. Note the narrow width of the concentration profile and hence the large gradients around the pore. Bearing in mind that typical open dwell times for single channels are a few milliseconds, (see e.g. [26, 27]) the profile almost instantaneously equilibrates on this time scale. A similar tendency can be observed in the current as depicted in the right panel of Figure 2. After an initial transient lasting a few microseconds, the current settles on a constant value.

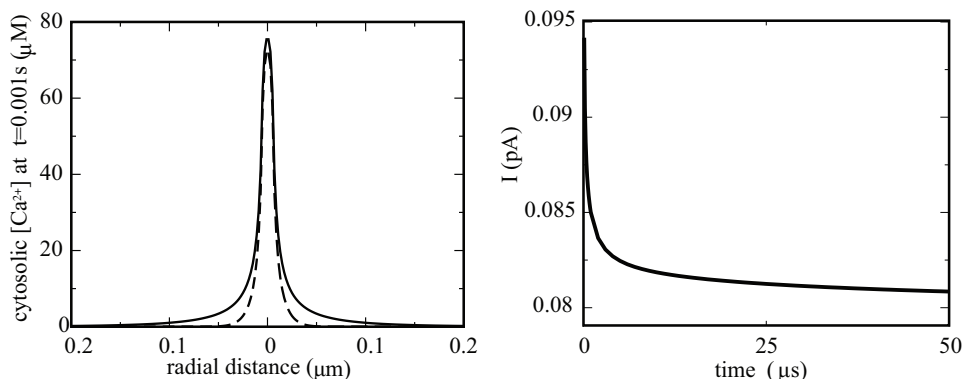


FIG. 2: Left: Spatial profile of free cytosolic Ca^{2+} $0.9 \mu\text{s}$ (dashed) and 1 ms (solid) after channel opening. Right: Single channel current in the first $50 \mu\text{s}$ upon channel opening. Parameter values as in Set 2 in Table I except

These results illustrate that the concentration of free Ca^{2+} around a conducting channel reaches values that are more than 3 orders of magnitude larger than resting concentrations in a cell. This difference will grow even further when we consider release through multiple channels in a cluster. Such orchestrated release, which is called a puff, raises the question whether it represents the sum of individual channels, or whether channels interact during Ca^{2+} liberation. We could consider channels to be independent if the depletion zone in the ER around a liberating channel is smaller than the distance between neighbouring channels. Our simulations reveal that the luminal concentration profile possesses a full width at half minimum of 10 nm after 15 ms. When we relate this to the inter-channel distance of approximately 12 nm as calculated by Swillens et al. [8], adjacent channels indeed interact. To account for such crosstalk, Swillens and co-workers demonstrated that the flux through mutually dependent channels corresponds to a flux through a single channel with a conducting area that equals the sum of the pore sizes of all individual channels. Hence, we set the area of a cluster with N_O open channels to $\pi N_O R_S^2$, which entails a cluster radius of $R = R_S \sqrt{N_O}$. Figure 3 shows the time evolution of concentration profiles of free cytosolic Ca^{2+} for different numbers of conducting channels at various distances from the cluster. The

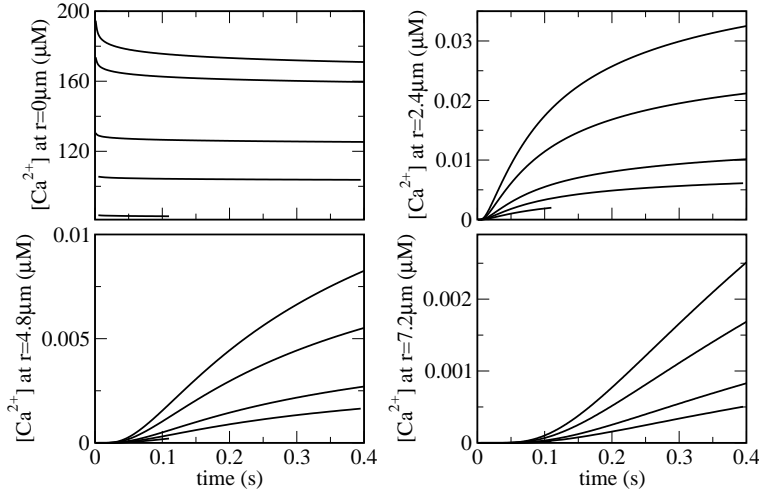


FIG. 3: Time dependence of the concentration profiles of cytosolic Ca^{2+} at different distances r from the channel cluster. Lines show results for 1, 2, 4, 11.11, and 21.77 open channels from lower to higher values. Release through a single channel was simulated for 0.115 s, all other release events lasted 400 ms. Note that all concentrations are increases above base level.

upper left panel depicts concentrations at the centre of the cluster. After initial transients,

concentrations remain constant at levels between approximately $100 \mu\text{M}$ and $170 \mu\text{M}$ for 2 to 21.77 releasing channels. The rational number of open channels is a consequence of the finite grid chosen for the simulations. Having fixed a certain number of grid points as radius R , the number of open channels follows from $N_O = R^2/R_S^2$ as outlined above. As for a single channel, we find here as well that profiles reach a steady state almost immediately. Moving away from the cluster, concentrations drop significantly. At a distance of $2.4 \mu\text{m}$ the strongest current produces concentrations of $\sim 30 \text{ nM}$ above base level only. Three times further away, the increase above base level lies in the nano-molar range. These results imply that firstly profiles of free cytosolic Ca^{2+} are strongly localised around a releasing cluster giving rise to very large gradients. Secondly, the increase of Ca^{2+} at neighbouring clusters is minute due to an inter-cluster distance of $2\text{--}7 \mu\text{m}$.

The large concentrations during a puff require us to reconsider earlier gating models of the IP_3 receptor as e.g. published in [12, 14, 28, 29]. There, state transitions of the receptor were coupled to bulk concentrations. However, averaged concentrations are 2–3 orders of magnitudes smaller than those experienced at a liberating cluster. Since transition rates in these models are directly proportional to the Ca^{2+} concentration, we will investigate the impact of such highly elevated Ca^{2+} concentrations on the dynamics of an IP_3R channel cluster in the next section.

III. Ca^{2+} PUFFS AND THE DETERMINISTIC GATING OF IP_3 RECEPTOR CHANNELS

The previous section focussed on properties of Ca^{2+} liberation through a constant number of open channels. Here, we would like to go a step further and include changes in the number of conducting channels during a Ca^{2+} puff. Our goal is to probe the response of deterministic gating models of the IP_3 receptor to localised concentration fields, since these models occupy a prominent spot in the ongoing study of intracellular Ca^{2+} . The focus on deterministic models entails that we will work with a release density rather than a discrete number of release channels. However, this transition does by no means correspond to a homogenisation of ion channels. In the spirit of Swillens et al. [8], we allow the size of the conducting membrane patch to vary between some maximal value, when all channels are open, and 0, when all channels are closed. Hence, Ca^{2+} release is still spatially restricted.

For the sake of computational convenience, we adapt a spherical geometry, so that the IP₃R channel cluster corresponds to a sphere of radius a that is centred in a larger sphere of radius b . The latter represents the cytosol. Let p denote the probability for a channel to be open, then the radius of the conducting cluster volume is given by $a = a_0\sqrt[3]{p}$, where a_0 corresponds to the maximal radius when all channels in the cluster are open. The third root stems from the fact the size of the conducting volume is proportional to the open probability. The functional form of p depends on the model of the IP₃ receptor. Here, we choose the one proposed by De Young and Keizer [12]. They argue that a single receptor expresses three binding sites: an activating IP₃ binding site, an activating Ca²⁺ binding site and an inhibiting Ca²⁺ binding site. The state of a receptor can hence be expressed by a binary triplet ijk where the first digit corresponds to the IP₃ binding site and the last two to the Ca²⁺ activating and Ca²⁺ inhibiting binding sites. An index equals 1 if an ion is bound and 0 otherwise. A receptor is deemed activated if IP₃ and Ca²⁺ are bound to their respective activating site, so that 110 represents the active state of the receptor. Let p_{ijk} denote the fraction of receptors in the state ijk , then the equations of motion for the set $\{p_{ijk}\}$ takes the form

$$\dot{p}_{ijk} = g_{ijk}(c, \{p_{ijk}\}), \quad i, j, k \in [0, 1], \quad (6)$$

where c refers to the cytosolic Ca²⁺ concentration. Note that equation (6) subsumes eight coupled equations. However, only seven of the eight variables are independent since probability is conserved, i.e.

$$\sum_{i,j,k=0}^1 p_{ijk} = 1. \quad (7)$$

Therefore, we only need to consider seven equations in (6). For the specific form of the functions g_{ijk} , we refer the reader to [12, 30]. To close equation (6), we have to specify the time evolution of the cytosolic Ca²⁺ concentration. In concurrence with the previous section, we set it to

$$\dot{c} = D\nabla_r^2 c + k_l(E - c) - k_p c + k_c(E - c)\Theta(a - r). \quad (8)$$

Here, the first term on the right hand side describes diffusion of Ca²⁺ governed by the Laplace operator ∇_r^2 in spherical co-ordinates. The remaining expressions correspond to a leak flux, SERCA pumps of strength k_p and Ca²⁺ release. The latter is restricted to the region $r \leq a$ by the Heaviside function Θ , which is 0 for negative arguments and otherwise

1. The linear SERCA pump model corresponds to a biophysical model [31] in the limit of no co-operativity and low affinity when luminal gating is neglected.

The value of $a = a_0\sqrt[3]{p}$ is usually time dependent because of the coupling to the open probability p . The value of p can be computed from properties of the IP₃ receptor channel. Early flux measurements [6, 32] revealed that an IP₃R channel consists of 4 receptors, and that the channel is conducting when at least 3 of the 4 receptors are activated. The tetrameric structure was recently confirmed by Jiang et al [22]. Therefore, we employ

$$a = a_0 p_{110} \sqrt[3]{4 - 3p_{110}}. \quad (9)$$

Equations (6), (8) and (9) form the dynamical system that describes Ca²⁺ liberation through a localised release site of time dependent size. To gain insight into how it responds to the large Ca²⁺ concentrations that we reported in the previous section, we perform a linear stability analysis. We begin with the stationary solutions to equations (6) and (8). The Heaviside function in equation (8) allows us to solve it separately for $0 \leq r < \bar{a}$ and $r \geq \bar{a}$. Throughout our analysis, an overbar indicates stationary values. We find the fixed point of the cytosolic Ca²⁺ concentration to be

$$\bar{c}(r) = B(\bar{a}) \frac{\exp(k_2(r - 2b)) - \exp(-k_2 r)}{r} \Theta(r - \bar{a}) + A(\bar{a}) \frac{\sinh(k_1 r)}{r} \Theta(\bar{a} - r), \quad (10a)$$

$$k_1^2 = \frac{k_l + k_p + k_c}{D}, \quad k_2^2 = \frac{k_l + k_p}{D}. \quad (10b)$$

The two unknowns A and B are determined by matching \bar{c} and its first derivative at \bar{a} . Turning back to the gating dynamics, a closer inspection of equation (6) reveals that the right hand side varies along the radial co-ordinate due to variations of c . Since the Ca²⁺ concentration does not vary significantly within a cluster, we decide to evaluate c at the boundary, which results in a unique set of gating variables p_{ijk} . With constant $\bar{c}(\bar{a})$, it follows from equation (6) that the stationary value for an active receptor is given by [33]

$$\bar{p}_{110} = \frac{d_2 \bar{c}(\bar{a}) I}{(\bar{c}(\bar{a}) + d_5)(d_1 d_2 + \bar{c}(\bar{a}) d_3 + \bar{c}(\bar{a}) I + d_2 I)}. \quad (11)$$

d_1 and d_3 denote the dissociation constant for IP₃ binding in the absence and presence of inhibitory Ca²⁺, respectively. The parameters d_2 and d_4 refer to dissociation constants for the inhibiting Ca²⁺ binding site depending on whether IP₃ is bound or not. The activating Ca²⁺ binding site is characterised by the dissociation constant d_5 , and I denotes the IP₃ concentration.

Up to now, the value of \bar{a} is still undetermined. However, inserting equation (11) into equation (9) and subsequently employing the expression for $\bar{c}(\bar{a})$ turns equation (9) into an implicit equation for \bar{a} . This concludes the computation of the stationary state.

We proceed by linearising equations (6) and (8) around the stationary solutions. Let y and δa be the perturbations of the Ca^{2+} concentration and the radius, respectively, then the linearised Ca^{2+} dynamics reads as

$$\dot{y} = D\nabla_r^2 y - (k_l + k_p)y - \Theta(\bar{a} - r)k_c y + k_c(E - \bar{c})\delta_D(r - \bar{a})\delta a, \quad (12)$$

where δ_D refers to Dirac's delta function. The perturbation δa follows from equation (9) as [33]

$$\delta a = \frac{\partial f}{\partial p_{110}} z_{110}(\bar{a}) \left[1 - \frac{\partial f}{\partial p_{110}} \frac{\partial \bar{p}_{110}}{\partial r} \right]^{-1}, \quad (13)$$

where z_{110} denotes the perturbation of the gating variable p_{110} around its equilibrium value. We used the short hand notation $f(p_{110}) = a_0 p_{110} \sqrt[3]{4 - 3p_{110}}$, and all partial derivatives in equation (13) have to be evaluated at $(\bar{c}(\bar{a}), \bar{p}_{110}(\bar{a}))$. A comparison of equation (12) with equation (8) reveals that the time dependent radius leads to an additional flux at the cluster edge. Once we make the ansatz $y(r, t) = u(r) \exp(\omega t)$ and linearise the gating dynamics, we find that the eigenvalue ω is determined by [33]

$$k_2 + k_1 \coth(k_1 \bar{a}) - \frac{k_c(E - \bar{c}(\bar{a}))}{D} \frac{\bar{a} \delta a}{\sinh(k_1 \bar{a})} = 0, \quad (14a)$$

with

$$k_1 = \sqrt{\frac{k_l + k_p + k_c + \omega}{D}}, \quad k_2 = \sqrt{\frac{k_l + k_p + \omega}{D}}. \quad (14b)$$

Hence, stability of the linearised Ca^{2+} profile is established by inspecting the real part of ω as a solution to equation (14a).

Before we present results for the stability analysis outlined above, we need to consider the choice of parameter values. The original De Young Keizer model was set-up and fitted to averaged Ca^{2+} concentrations. Since they result from a homogeneous release density, the release strength k_c^{DK} estimated by De Young and Keizer has to be re-scaled to accommodate for localised Ca^{2+} liberation. Let L be a typical inter-cluster distance, then we set $a_0^3 k_c = L^3 k_c^{DK}$. This relation assures flux conservation between the two models, because there is one localised cluster of volume a_0^3 for every volume L^3 in the homogeneous model. This scaling results in $k_c = 34500 \text{ s}^{-1}$, which is close to realistic values [20]. Other critical parameters

are the dissociation constants, as they measure the sensitivity of the binding and unbinding processes.

The impact of the dissociation constant for Ca^{2+} activation is illustrated in Figure 4. It depicts the IP_3 concentration for a Hopf Bifurcation and two saddle node bifurcation in dependence on d_5 . The Hopf bifurcation occurs always at higher values of d_5 than both saddle node bifurcations. All three bifurcations coalesce in a cusp at approximately $0.375 \mu\text{M}$. Below this point, only a single linearly stable fixed point exists. Taking into account that experimentally reported values for d_5 range between 77 nM [26] and 330 nM [34] (De Young and Keizer employed 82.34 nM), oscillations do not occur for measured dissociation constants d_5 in the presence of localised Ca^{2+} release.

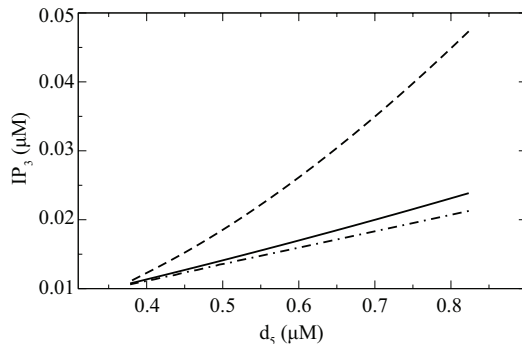


FIG. 4: IP_3 concentration of the saddle node bifurcations (solid and dashed dotted) and the Hopf bifurcation (dashed) in dependence on d_5 . Parameters values are $d_1 = 0.13 \mu\text{M}$, $d_2 = 3 \mu\text{M}$, $d_3 = 0.9434 \mu\text{M}$, $d_4 = 0.4133 \mu\text{M}$, $k_p = 80 \text{ s}^{-1}$, $k_l = 0.002 \text{ s}^{-1}$, $k_c = 34500 \text{ s}^{-1}$, $E = 750 \mu\text{M}$, $a_0 = 0.03 \mu\text{M}$, $D = 40 \mu\text{m}^2\text{s}^{-1}$.

The only way to induce Ca^{2+} oscillations in this deterministic framework is the use of unphysiologically high values of d_5 . But even then, these oscillations could never be observed in experiments. Figure 5 provides a first evidence. It shows bifurcation diagrams for two different values of the Ca^{2+} diffusion coefficient representing buffered diffusion (left panel) and free diffusion (right panel). A single fixed point exists for most values of the IP_3 concentration. Two saddle node bifurcation occur at small values of I , and a Hopf bifurcation gives rise to oscillations on the upper branch. These persist from the Hopf bifurcation towards smaller values of the IP_3 concentration and vanish in a putative homoclinic bifurcation close to the lower saddle node point. Hence, oscillations occur only in a restricted range of IP_3

concentrations, which is too small to be of experimental relevance.

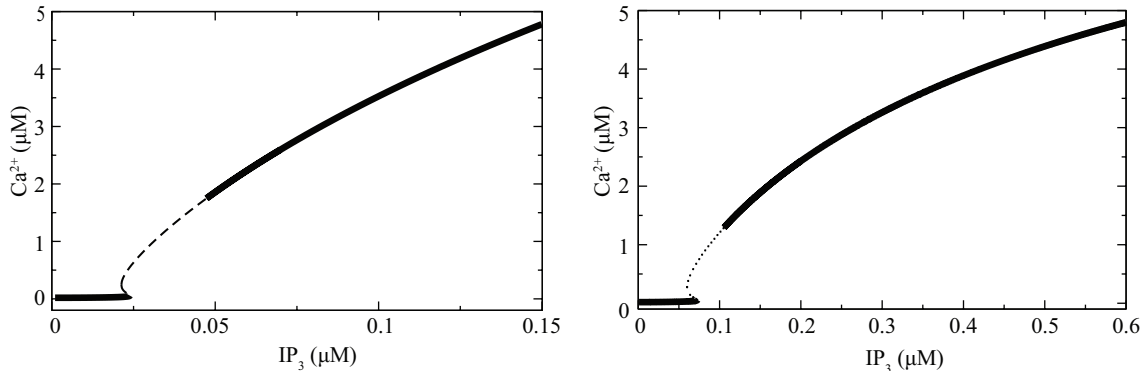


FIG. 5: Stationary values of the Ca^{2+} concentration for $D = 40 \mu\text{m}^2\text{s}^{-1}$ (left) and $D = 220 \mu\text{m}^2\text{s}^{-1}$ (right) computed from equation (10a) at $r = \bar{a}$. Solid lines denote linearly stable fixed points, dashed and dotted lines denote linearly unstable points. Parameters as in Figure 4 and $d_5 = 0.8234 \mu\text{M}$.

The characteristics of the oscillations as shown in Figure 6 corroborate our idea even further. The left panel depicts oscillations at the centre of the releasing cluster. After an initial transient, which illustrates that we indeed reach realistic values of the Ca^{2+} concentration at a cluster, the Ca^{2+} dynamics settles into small amplitude oscillations. Moving away from the cluster reduces the amplitude considerably. At a distance of $1.588 \mu\text{m}$, the Ca^{2+} concentration changes less than a nanomolar. These oscillations are too small to be measured, and hence cannot represent observed global oscillations.

When we probe the parameter space even further, the topology of the bifurcation diagram changes significantly. Instead of two saddle node points as in Figure 5, only one saddle node bifurcation occurs as illustrated in Figure 7. Beyond the Hopf bifurcation on the upper branch, two stable solutions exist and extend infinitely towards larger values of the IP_3 concentration.

Moreover, we discovered a period doubling sequence, which suggests that oscillations might not only vanish due to a (putative) homoclinic bifurcation. Figure 8 demonstrates that decreasing the IP_3 concentration gives rise to a period-2 and then to a period-4 solution. As for the regular oscillations discussed above, these closed orbits only exist for a small range of IP_3 concentrations and the amplitude of the oscillations is again considerably damped when moving away from the cluster [33].

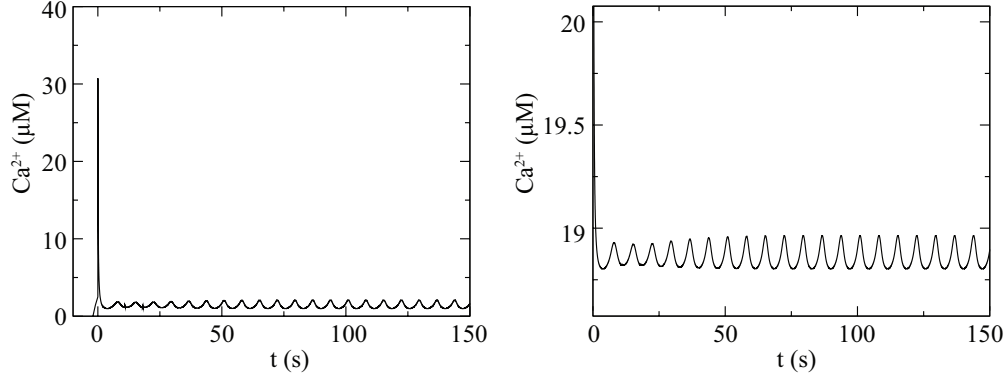


FIG. 6: Oscillation of the Ca^{2+} concentration at $r = 0 \mu\text{m}$ (left) and $r = 1.588 \mu\text{m}$ (right). Note the difference in the order of magnitude for the amplitude and mean. Parameters as in Figure 5 and $D = 40 \mu\text{m}^2\text{s}^{-1}$, $a_2 = a_4 = 0.2 (\mu\text{Ms})^{-1}$, $a_5 = 1 (\mu\text{Ms})^{-1}$.

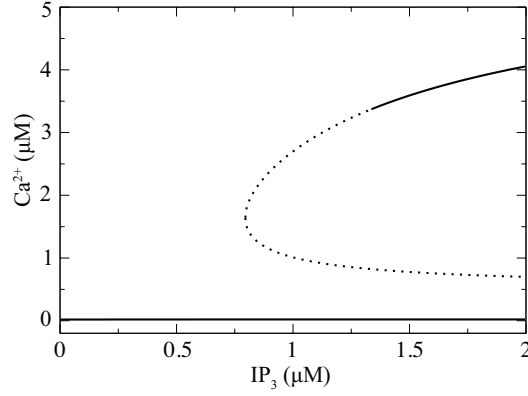


FIG. 7: Stationary values of the Ca^{2+} concentration for $D = 220 \mu\text{m}^2\text{s}^{-1}$ computed from equation (10a) at $r = \bar{a}$. Solid lines denote linearly stable fixed points, dotted lines linearly unstable fixed points. Parameter values are $d_1 = 0.13 \mu\text{M}$, $d_2 = 12.588 \mu\text{M}$, $d_3 = 0.9434 \mu\text{M}$, $d_4 = 1.7346 \mu\text{M}$, $d_5 = 2.4702 \mu\text{M}$, $k_p = 80 \text{ s}^{-1}$, $k_l = 0.002 \text{ s}^{-1}$, $k_c = 700 \text{ s}^{-1}$, $E = 750 \mu\text{M}$, $a_0 = 0.11 \mu\text{m}$, $a_2 = a_4 = 0.0167 (\mu\text{Ms})^{-1}$, $a_5 = 0.667 (\mu\text{Ms})^{-1}$.

The reason for the absence of oscillations at experimentally supported parameter values lies in the saturation of all feedback processes. The highly elevated Ca^{2+} concentrations at a cluster are orders of magnitude larger than any dissociation constants, and hence deterministic gating mechanisms have already reached their maximal response. Since this behaviour is often characterised by an extended plateau — as is the case for frequently used Hill functions — no feedback can be exerted anymore. The only way to reintroduce

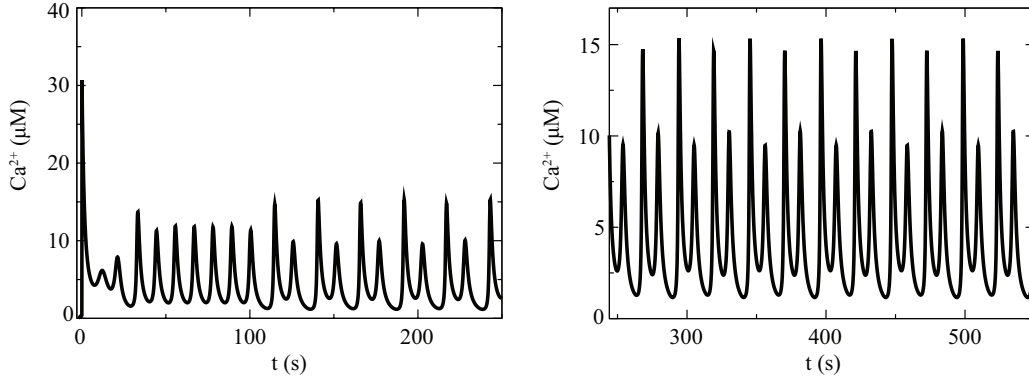


FIG. 8: Oscillations of the Ca^{2+} concentration at $r = 0 \mu\text{m}$ for different values of the IP_3 concentration. At $t = 100 \text{ s}$, we decreased I from $0.22 \mu\text{M}$ to $0.218 \mu\text{M}$ (left panel), whereas $I = 0.215 \mu\text{M}$ for all times in the right panel. Parameter values as in Fig 7 and $D = 50 \mu\text{m}^2\text{s}^{-1}$.

oscillations into localised Ca^{2+} release is to allow for fluctuations. These fluctuations arise from the small number of channels per cluster. The state of a cluster does not change smoothly, but jumps in response to changes in single channels. These alterations arise from random association and dissociation of Ca^{2+} and IP_3 at their regulatory sites. Hence, we need to extend the description of gating dynamics from deterministic equations to the field of stochastic processes.

IV. A MASTER EQUATION APPROACH TO Ca^{2+} PUFF DYNAMICS

The insight that fluctuations constitute the driving force behind intracellular Ca^{2+} oscillations necessitates a change in perspective. The dynamics of a cluster does not depend on averaged properties of a large number of ion channels, but it is the behaviour of individual channels that determines any response. This holds especially true for the initiation of a Ca^{2+} puff. It is the transition of a single channel to the open state in a background of closed channels that sets off Ca^{2+} liberation. Therefore, the essential ingredient to quantify the beginning of a puff is the probability of an individual channel to open between t and $t + dt$ when the Ca^{2+} concentration is at base level.

Single channel properties like this have been studied extensively in the past, and powerful methods have been developed to characterise the stochastic behaviour of plasma membrane ion channel [35, 36]. However, the large number of states of a single IP_3R channel, which can

range between 330 and 1800 depending on the receptor model, requires different approaches. This holds especially true for the computation of the transition probability to the open state. In general, the calculation of this probability depends on the morphology of the ion channel. In case of the IP₃R channel, there are 4 receptors per channel, and as pointed out earlier, the channel is conducting when at least 3 of the 4 receptors are activated. Given a specific receptor model, there might be more than one configuration of all four receptors in the open state of the channel. Consider for a moment the De Young Keizer model and the situation when 3 of the 4 receptors are activated. Then 3 receptors are in the state 110, but the fourth can be in any other of the 8 receptor states except 110. Since the four receptors are deemed independent and indistinguishable, combinatorial analysis yields 7 distinct receptor configurations that correspond to this open channel state.

Before we address the general case of multiple receptor configurations, we take a step back and consider an ion channel where all receptors need to be in the activated state A for the channel to be open. Hence, there is exactly one conducting configuration in terms of receptor states. The last transition before the channel opens is therefore the one where all but one receptor are in the activated state. This entails that up to this point any of the receptors can have visited the activated state A arbitrarily often, so that the probability density for a channel is not a power of the single receptor probability density.

The notion of arriving in the activated state links the activation of a channel to first passage time problems. Generally, let $q(X, t|Y, \tau)$ denote the probability of the channel to be in the state X at time t when it was in the state Y at time τ , and $F(X, t|Y, 0)dt$ the probability of arriving in the state X for the first time in the interval $[t, t + dt]$ when the initial state was Y . Then these two quantities satisfy the relation [37]

$$q(X, t|Y, 0) = \delta_{X,Y}\delta(t) + \int_0^t d\tau q(X, t|X, \tau)F(X, \tau|Y, 0). \quad (15)$$

The probability of being in X at time t equals the probability of arriving there for the first time in some interval $[\tau, \tau + d\tau]$, $\tau \leq t$, times the probability of being in X at time t given the initial condition (X, τ) . The integral sums over all τ between 0 and t , and the delta functions take care of initial values. In the case of a time-homogeneous process, $q(X, t|Y, \tau) = q(X, t - \tau|Y, 0)$ [38], so that the Laplace transform of equation (15) for $X \neq Y$ readily follows as

$$\hat{q}(X, s|Y, 0) = \hat{F}(X, s|Y, 0)\hat{q}(X, s|X, 0). \quad (16)$$

Since $F(X, t|X, 0) = \delta(t)$, we finally obtain

$$\hat{F}(X, s|Y, 0) = \frac{\hat{q}(X, s|Y, 0)}{\hat{q}(X, s|X, 0)} (1 - \delta_{X,Y}) + \delta_{X,Y}. \quad (17)$$

The feasibility of the Laplace back-transform to compute $F(X, t|Y, 0)$ depends crucially on the functional form of \hat{q} . To construct the latter, we first focus on the dynamics of a single receptor. Since the following derivation holds for any receptor model, we consider a receptor with n states and any transitions between them. Bearing in mind that these transitions are stochastic as they derive from chemical interactions, we describe them by a master equation [38, 39]. Let P be a vector that contains the probabilities $p(i, t|j, 0)$ to be in the receptor state i at time t with initial state j , i.e. $P(t|j, 0) = (p(1, t|j, 0), \dots, p(n, t|j, 0))$, then the dynamics of P is governed by $d_t P(t|j, 0) = W P(t|j, 0)$. The elements w_{ij} of the matrix $W \in \mathbb{R}^{n \times n}$ correspond to transition rates from the receptor state j to the receptor state i . All diagonal elements w_{ii} are such that each column sums to 0. For a time independent matrix W that can be diagonalised, a solution of P reads as

$$P(t|j, 0) = \sum_{i=1}^n c_{ji} V_i \exp(\lambda_i t). \quad (18)$$

The coefficients $c_{ji} \in \mathbb{R}$ are determined by initial conditions. $\lambda_i \in \mathbb{R}$ and $V_i = (v_{1i}, \dots, v_{ni})$ denote an eigenvalue and the corresponding eigenvector of W , respectively.

Having established the probability for a single receptor, we can incorporate equation (18) into a channel state. Let there be h independent receptors per cluster [24], then the probability to be in the activated channel state A at time t given some initial state I at time 0 follows as

$$q(A, t|I, 0) = \prod_{i=1}^n p(a, t|i, 0)^{m_i} = \prod_{i=1}^n \left(\sum_{j=1}^n c_{ij} v_{ja} \exp(\lambda_j t) \right)^{m_i}. \quad (19)$$

The initial state is such that m_i receptors are in state i , $i = 1, \dots, n$. Some algebra and combinatorial analysis reveal that equation (19) can be cast into the compact form [40]

$$q = \sum_{j=1}^r M_j(\{m_i\}) \exp(\eta_j t), \quad (20)$$

where η_j is a linear combination of eigenvalues of W , and the constants M are determined by initial conditions. The upper limit $r = \binom{h+n-1}{n-1}$ counts the number of ways to distribute h receptors on n receptor states. We can immediately compute the Laplace transform of

equation (20), which yields

$$\hat{q}(A, s|I, 0) = \sum_{j=1}^r \frac{M_j(m)}{s - \eta_j}. \quad (21)$$

Since the common denominator is independent of initial conditions, it cancels when we insert equation (21) into equation (17), so that we find

$$\hat{F}(A, s|I, 0) = \frac{\hat{q}(A, s|I, 0)}{\hat{q}(A, s|A, 0)} = \frac{\tilde{q}(A, s|I, 0)}{\tilde{q}(A, s|A, 0)}, \quad I \neq A, \quad (22)$$

with $\tilde{q}(A, s|I, 0) = \sum_j M_j(m) \prod_{k \neq j} (s - \eta_k)$. Consequently, the first passage time density in the time domain follows readily as

$$F(A, t|I, 0) = \sum_{j=1}^{r-1} \frac{\tilde{q}(A, s_j|I, 0)}{\tilde{q}'(A, s_j|A, 0)} \exp(s_j t), \quad I \neq A, \quad (23)$$

using contour integration. The prime indicates the derivative with respect to s , and $\{s_j\}$ is the set of all zeros of $\tilde{q}(A, s|A, 0)$.

Equation (23) allows us to quantify the initiation of a Ca^{2+} puff if each channel in a cluster possesses a unique open state in terms of its receptor states. However, the multimeric structure of ion channels often leads to more than one conducting state, as we discussed for the IP_3R channel earlier. This requires us to generalise our previous derivation to r_a open channel states A_i , $i = 1, \dots, r_a < r$, so that the overall conducting state is given by $A = \sum_i A_i$. Let $F(A_i A, t|I, 0) dt$ denote the probability to arrive in the open state A_i for the first time without having visited any of the other active states A_j , $j \neq i$, given some initial state I at time 0. Since all A_i are mutually exclusive, the probability to initiate a puff in the interval $[t, t + dt]$ follows as $F(A, t|I, 0) = \sum_i F(A_i A, t|I, 0)$ [41]. This leads us directly to a generalisation of equation (15)

$$q(A_i, t|I, 0) = \delta_{A_i, I} \delta(t) + \sum_{j=1}^{r_a} \int_0^t d\tau F(A_j A, \tau|I, 0) q(A_i, t|A_j, \tau), \quad (24)$$

$i = 1, \dots, r_a$, which is equivalent to

$$\hat{q}(A_i, s|I, 0) = \sum_{j=1}^{r_a} \hat{F}(A_j A, s|I, 0) \hat{q}(A_i, s|A_j, 0), \quad (25)$$

for $I \neq A_i$. Equation (25) is a system of r_a equations for the r_a unknowns $\hat{F}(A_j A, s|I, 0)$, which can be solved by standard techniques as demonstrated in [40]. Note that $\hat{F}(A_j A, s|I, 0)$ are fractions of polynomials and hence can be Laplace back-transformed in analogy with

equation (22). The left panel in Figure 9 illustrates that results from our analytical approach are almost indistinguishable from stochastic simulations. We used the transition matrix

$$W_3 = \begin{pmatrix} -6 & 10 & 12 \\ 2 & -15 & 3 \\ 4 & 5 & -15 \end{pmatrix}. \quad (26)$$

Having first passage time densities at the channel level at our disposal, we can now move on to a cluster with N channels. This raises the question of how to specify initial cluster states. On the one hand, we could prescribe the numbers $\{b_i\}$ of subunits in state i , $i = 1, \dots, n$, and then distribute them onto all hN subunits. However, the mere number of subunits does not uniquely fix the cluster state in terms of channel states, as rearrangement of subunits between different channels can result in different channel states. Let $\{u\} = (u_1, \dots, u_r)$, $\sum_i u_i = N$, denote an arbitrary, but fixed collection of channel states that complies with the set $\{b_i\}$. Then, the probability for a cluster to be activated is given by

$$F_{\{u\}}(t) = \sum_{i=1}^r u_i F(A, t|I_i, 0) G^{u_i-1}(A, t|I_i, 0) \prod_{j \neq i} G^{u_j}(A, t|I_j, 0), \quad (27)$$

with

$$G(A, t|I_i, 0) = 1 - \int_0^t F(A, \tau|I_i, 0) d\tau. \quad (28)$$

$G(A, t|I_i, 0)$ is the probability that a channel that was originally in the i th channel state has not yet been activated at time t . Note that $G(A, t|A, 0) = \delta(t)$. Equation (27) states that a cluster is activated for the first time when one channel opens for the first time while all other channels are still closed. Since equation (27) represents only one specific channel configuration, we obtain the first passage time density for a cluster by averaging over all set of channel states $\{u\}$ that can be derived from the subunit collection $b = \{b_i\}$, i.e. [40]

$$\bar{F}_b(t) = \langle F_{\{u\}}(t) \rangle_{u|b}. \quad (29)$$

The right panel in Figure 9 illustrates this procedure for a cluster of 7 trimeric channels, where the subunit transition matrix W is given by

$$W_4 = \begin{pmatrix} -15 & 2 & 0 & 3 \\ 5 & -4 & 3 & 0 \\ 0 & 2 & -9 & 3 \\ 10 & 0 & 6 & -6 \end{pmatrix}. \quad (30)$$

The analytical approach is in an excellent agreement with direct stochastic simulations.

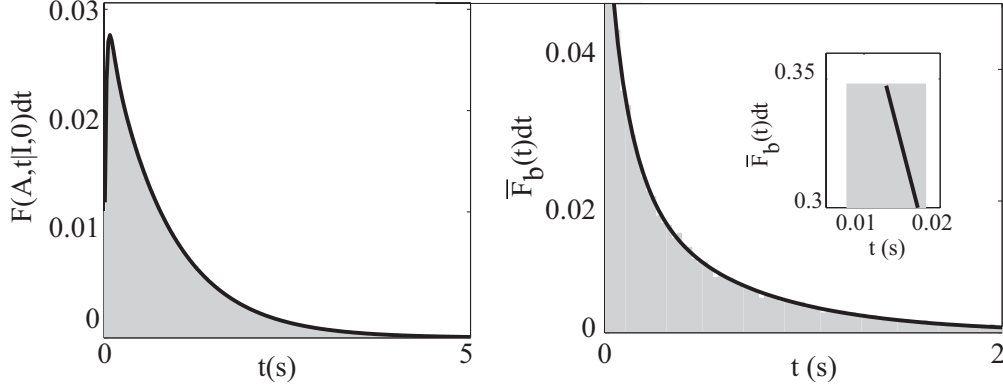


FIG. 9: Left: Escape probability F for a channel with 3 3-state subunits using eqs. (23) and (25). The initial state is $I = (0, 0, 3)$, and the absorbing state is $A = (0, 2, 1) \cup (1, 2, 0)$. Right: Escape probability \bar{F}_b for a cluster of 7 trimeric channels. Each subunit is modelled by 4 states. 10 is the activated state of the subunit. Initial conditions are $(n_{00}, n_{10}, n_{11}, n_{01}) = (2, 8, 4, 7)$, and the absorbing state is when a channel has 3 subunits in 10 for the first time. The inset shows a blow up of the delta-peak at $t = 0$. Lines - analytic results, shaded areas - histograms from stochastic simulations (500000 trials).

Another way to assign an initial cluster state is in terms of the probability $o(i)$ of a single subunit to be in state i initially. Then,

$$F_{ch}(t) = \sum_{j=1}^r \frac{h!}{m_{1j}! \dots m_{nj}!} \prod_{i=1}^n o(i)^{m_{ij}} F(A, t | I_j, 0), \quad (31)$$

where I_j indicates the j th channel state as initial condition given and m_{ij} represents the number of subunits in the state i given the j th channel state ($\sum_i m_{ij} = h$). $F_{ch}(t)$ corresponds to a distribution averaged over all initial conditions. The probability density for a cluster to be activated for the first time is in this formulation

$$F_{cl}(t) = N F_{ch}(t) G_{ch}^{N-1}(t), \quad (32)$$

with

$$G_{ch}(t) = 1 - \int_0^t F_{ch}(\tau) d\tau. \quad (33)$$

A fundamental difference between equation (29) and equation (32) is that the first one requires numbers of subunits as input, whereas the latter is based on probabilities. Nevertheless, they are closely related. When we choose probabilities $o(i)$, then a specific initial configuration b of subunits is sampled with a probability

$$p(\{b\}) = \frac{(Nh)!}{b_1! \dots b_n!} \cdot \prod_{i=1}^n o(i)^{b_i}. \quad (34)$$

Hence, the relation between the two first passage time densities is given by

$$F_{cl}(t) = \sum \bar{F}_{\{b\}}(t) p(\{b\}). \quad (35)$$

The left panel of Figure 10 illustrates this concept. Originally, equations (29) and equation (32) yield different probability densities, but the scaling in equation (35) transforms one into the other. The right panel of Figure 10 shows that there is almost no difference between the application of equation (34) and statistics obtained from stochastic simulations.

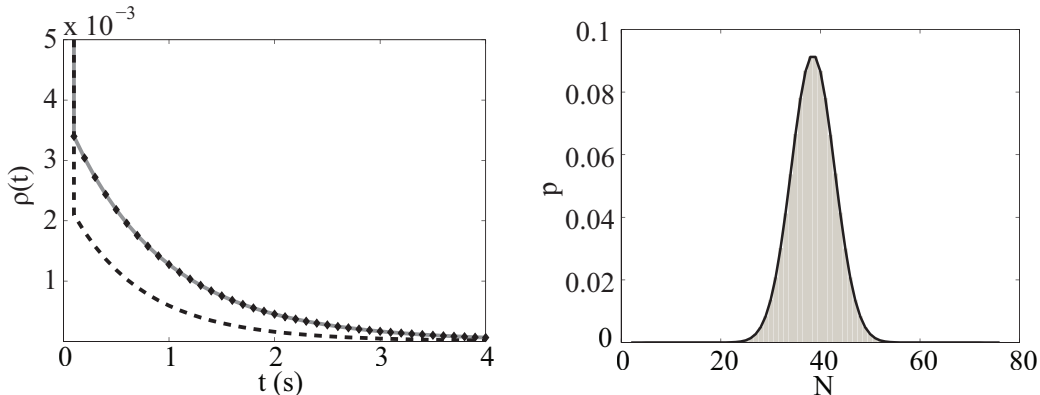


FIG. 10: Left: Comparison between equation (29) (dashed line) for initial conditions (37, 38) and equation (32) (diamonds) for $(p_o, p_c) = (0.5, 0.5)$. The discrepancy is resolved by equation (35) (grey solid line). Right: Distribution of initial number of activated subunits for $(p_o, p_c) = (0.5, 0.5)$ from stochastic simulations (bars) and evaluated from a binomial distribution (solid line). All computations are performed for a cluster of 25 trimeric channels, of which each subunit is modelled by two states with transition rates $r = g = 0.1 \text{ s}^{-1}$.

So far, our approach was based on the master equation of a single receptor, from which we constructed first channel and then cluster dynamics. The advantage of this method is that usually the number of receptor states is small. Hence, the ensuing master equation presents

a low dimensional ordinary differential equation, for which it is computationally cheap to evaluate all eigenvalues and eigenvectors. The highest computational costs arise for the Laplace back-transform, as we have to find all zeros $\{s_i\}$ of a large order polynomial [40]. We can alleviate the complexity of the last step by directly constructing the master equation for a channel. The price we pay is to analyse a high dimensional master equation because there are r channel states as defined after equation (20) in contrast to only n receptor states. However, such a shift of computational load can be beneficial [42].

To derive the channel master equation, we first construct the transition probabilities p_{ij} to move from channel state j to channel state i in the infinitesimal time interval dt . Since we still assume that only a single binding site can change state in an each epoch dt , the transition probability is zero between channel states for which the number of receptors in any receptor state differs by more than one. Otherwise we have $p_{ij} = \phi w_{kl}$ if a transition from receptor state l to state k corresponds to a change in channel state from j to i and there are ϕ receptors in state l .

We pointed out earlier that there might be more than one activated channel state A_i , $i = 1, \dots, r_a$. Given some initial channel state I , we obtain the probability to arrive in any of the activated states A_i for the first time by solving the channel master subject to the condition $q(A_i, t|I, 0) = 0$ for all $t \geq 0$ [38]. Such absorbing boundary conditions in state space entail that we can delete all lines and rows in the transition matrix $P = p_{ij}$ that correspond to the activated states. This leaves us with the master equation $\dot{y} = \tilde{P}y$, where $y = \{q(X, t|I, 0) | X \neq A_i\}$ and hence $\tilde{P} \in \mathbb{R}^{r-r_a \times r-r_a}$. Let $f(A, t|I, 0)$ be the probability that the channel is activated in the interval $[0, t]$ then

$$f(A, t|I, 0) = 1 - \sum_{X \neq A_i} q(X, t|I, 0) = 1 - \sum_{i=1}^{r_a} \sum_{j=1}^{r_a} c_j V_{ji} e^{\lambda_j t}, \quad (36)$$

where λ_j and $V_j = V_{ji}$ denote the eigenvalues and eigenvectors of \tilde{P} , respectively. The coefficients c_j are determined by initial conditions. From equation (36), the probability for a channel to open for the first time in the interval $[t, t + dt]$ then follows as

$$F(A, t|I, 0) = \frac{d}{dt} f(A, t|I, 0) = - \sum_{i=1}^{r_a} \sum_{j=1}^{r_a} c_j \lambda_j V_{ji} e^{\lambda_j t}. \quad (37)$$

A comparison of equation (37) to (23) shows that the eigenvalues of \tilde{P} correspond to the set of zeros $\{s_i\}$.

All cluster properties readily follow from equations (32) and (33) because initial conditions are defined in terms of channel states and not with respect to receptor states. Figure 11 shows results for the first passage time probabilities of a cluster when we apply three different models for the IP₃ receptor. Firstly, we investigated a nine-state model suggested in [43, 44], which we reduced to an eight state model. The second model is a variation of the first one that takes into account sequential binding as proposed by Taylor and Adkins [45]. The last implementation foots on work by Sneyd et al [29] with modifications suggested in [46] and studied in [47]. For more details, we refer the reader to [42]. All three plots demonstrate excellent agreement between our analytical approach and direct stochastic simulations. Initial conditions are sampled according to the equilibrium channel state distribution, which corresponds to the eigenvector associated with the zero eigenvalue of P .

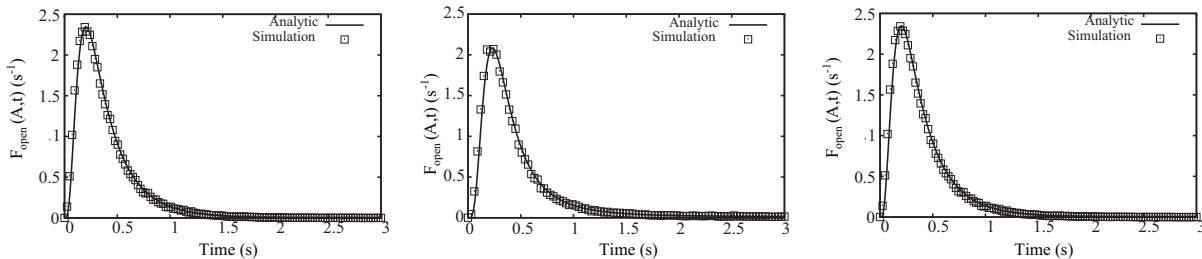


FIG. 11: First passage time probability density F for a cluster of 5 tetrameric IP₃ channels for different receptor models. Each receptor is based on [43, 44] (left), [45] (middle) and [29] (right). See text for details. Parameter values are listed in Table II for the left and middle panel except $a_2 = a_5 = 10^{-3} (\mu\text{Ms})^{-1}$, $b_2 = 0.016 \text{ s}^{-1}$ and $b_5 = 8 \cdot 10^{-4} \text{ s}^{-1}$ for the middle panel. Table III shows parameter values for the right panel.

With the probability distribution for Ca^{2+} puff initiation at our disposal, we are now in the position to analyse whole cell signals. Recent measurements in various cell types [48, 49] have revealed that global Ca^{2+} oscillations are stochastic. In the next section, we address the question whether such random behaviour at the cell level can indeed be caused by fluctuations at the cluster level.

V. GLOBAL CALCIUM OSCILLATIONS

A trademark of global Ca^{2+} oscillations is the orchestrated action of Ca^{2+} puff sites in a cell. The degree of recruitment during a single transient varies with cell size, so that almost all Ca^{2+} puff sites respond in smaller cells, but a lower ratio of clusters may be involved in larger cells. Recent experiments in small cancer cells revealed the expression of less than 10 puff sites [50]. Inspired by these findings, we here consider a cell with 8 clusters. They are arranged at the vertices of a cube of edge length d , which is embedded in a larger sphere. The dynamics of the cytosolic Ca^{2+} concentration is governed by a variation of equation (8), i.e.

$$\dot{c} = D\nabla^2 c - k_p c + \sigma \sum_i^* \delta(r - r_i), \quad (38)$$

where the asterisk indicates a summation restriction to conducting clusters only. Puff sites are located at positions r_i , and σ denotes the release strength of a liberating cluster. For computational convenience, we set σ to a constant value that does not depend on the number of open channels per cluster, although future implementations will use a more sophisticated approach [51]. Based on a single channel current of 0.2 pA [52] and the assumption of three open channels per puff, we estimate $\sigma \approx 3000 \mu\text{mols}^{-1}$. Note that the unit of σ follows from our choice of measuring concentrations in μM , space in μm and time in s. We demonstrated in Section II that concentration profiles around a liberating cluster equilibrate fast on the time scale of release. Hence, we performed a quasi steady-state analysis of equation (38), so that the increase of Ca^{2+} at a closed cluster positioned at r_j is given by

$$c_j = \frac{\sigma}{D} \sum_i^* \frac{\exp(-\lambda|r_j - r_i|)}{4\pi|r_j - r_i|}, \quad \lambda = \sqrt{\frac{k_p}{D}}, \quad (39)$$

where the spatial dependence results from the Green's function of the Helmholtz equation [53]. The Ca^{2+} concentration at an open cluster readily follows as

$$c_i^o = \frac{\sigma \exp(-\lambda a)}{D 4\pi a}, \quad (40)$$

where a corresponds to a typical cluster radius. We describe the initiation of Ca^{2+} release at a closed cluster by waiting time densities $F(A, t - t')$ as derived in Section IV. These distributions are always computed from the actual Ca^{2+} concentration at the quiescent puff site, and t' refers to the time of the last concentration change within the entire cell. Since we are interested in Ca^{2+} oscillations, we need to consider a mechanism by which channels

close. Under the assumption that we may treat termination of release as a cluster property rather than at the level of single channels, we employ a Poisson process with IP_3 dependent rate $\mu(I)$ for this purpose. Hence, the probability density for a cluster to close reads as

$$F_{cl}(I) = \mu(I)e^{-\mu(I)t}. \quad (41)$$

As the Ca^{2+} concentration around a conducting cluster is highly elevated in comparison to base level concentrations c_0 , we use a closing rate that is independent of c_0 . The dependence on the IP_3 concentration follows from the experimental observation that the open probability of IP_3R channels increases with rising IP_3 concentrations. The larger number of channels that can open at higher IP_3 concentrations translates into a monotonically decreasing behaviour of $\mu(I)$.

Putting opening and closing distributions together, we simulated whole cell responses using a recent hybrid algorithm [54]. Figure 12 illustrates that global Ca^{2+} oscillations can indeed arise from local Ca^{2+} puff dynamics. As observed in experiments, there is a clear division between Ca^{2+} puffs and Ca^{2+} oscillations. In the latter, seven and eight clusters participate, since as soon as more than one Ca^{2+} puff occurs in a small time window, the Ca^{2+} concentration at adjacent clusters increases to such an extent as to facilitate channel opening. Moreover, the stochastic nature of global Ca^{2+} oscillations is clearly visible.

VI. CONCLUSION

A quantitative understanding of intracellular Ca^{2+} signals ultimately starts from the basic building block of all cellular Ca^{2+} patterns: Ca^{2+} puffs and Ca^{2+} sparks. In the study at hand, we focussed on Ca^{2+} puffs, which refer to Ca^{2+} liberation through IP_3 receptor channels. Experiments have provided strong evidence that the IP_3R channel does not only release Ca^{2+} , but its gating dynamics strongly depends on Ca^{2+} levels in both the cytosol and the lumen (see e.g. [55, 56]). Therefore, we first investigated the range of Ca^{2+} concentrations that occur at a releasing cluster. We performed simulations in a three dimensional geometry that mimics the local environment of a cluster. Importantly, we took into account that a cluster possesses a finite radius (i.e. is not a point source) and that adjacent clusters are far away in terms of the diffusion length of intracellular Ca^{2+} . Hence, Ca^{2+} liberation is a spatially confined process. We found that peak concentrations at a cluster reach up to

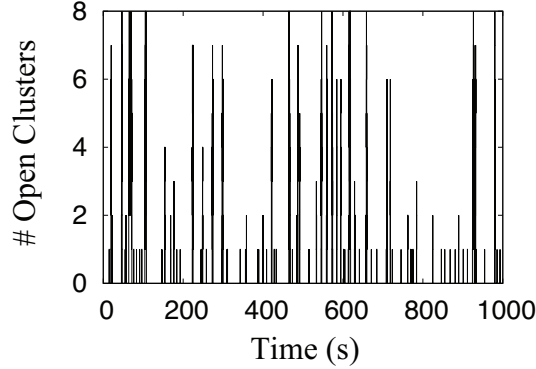


FIG. 12: Stochastic simulation of global Ca^{2+} oscillations based on local Ca^{2+} puff dynamics. Each cluster contains five tetrameric channels, and each receptor is based on the De Young Keizer model [12]. One open cluster corresponds to a Ca^{2+} puff, larger numbers of open clusters indicate a global oscillation. Parameter values are $c_0 = 0.03 \mu\text{M}$, $\text{IP}_3 = 1 \mu\text{M}$, $\mu = 5.5 \text{ s}^{-1}$, $\sigma = 3000 \mu\text{mols}^{-1}$, $D = 220 \mu\text{m}^2\text{s}^{-1}$, $k_p = 80 \text{ s}^{-1}$ and $d = 1.5 \mu\text{m}$. See Table IV for parameter values of the De Young Keizer model.

approximately $170 \mu\text{M}$ for 22 open channels, while a single channel still gives rise to almost $80 \mu\text{M}$. These concentrations are 2–3 orders of magnitude larger than bulk concentrations. Moreover, concentration profiles decay rapidly around a cluster. In a distance of $2.4 \mu\text{m}$, the strongest current leads to an increase of $\sim 30 \text{ nM}$ above base level only, which reduces to less than 3 nM at a range of $7.2 \mu\text{m}$.

These findings have significant consequences for both single cluster dynamics and cluster-cluster coupling. The impact on the latter is revealed through the amplification of the open probability of IP_3R channels in nearby clusters bearing in mind that an increase in cytosolic Ca^{2+} results in a larger open probability. An excess of a few nanomolar delivered from one cluster might not be enough to raise the open probability significantly. Hence, a single Ca^{2+} puff is most likely unable to initiate a propagating Ca^{2+} wave as it cannot induce activity in adjacent clusters. The beginning of a wave requires a minimum number of Ca^{2+} puffs in close proximity and hence represents a nucleation process.

At the single cluster level, the dynamics of IP_3 receptors is subject to the highly elevated local Ca^{2+} concentrations. Given that binding and unbinding of Ca^{2+} influences the state of a receptor, these state changes are driven by much larger concentrations than previously recognised. However, most of the modelling work in the past foots on averaged concentra-

tions. The existence of global oscillations was predicted based on bulk concentrations, as was the computation of frequencies and amplitudes. In the light of our new results, shadows fall on the validity of these findings. Hence, we investigated the behaviour of the De Young Keizer model [12] as one of the prototypical frameworks of the IP_3 receptor under the influence of localised concentration fields.

In a three dimensional geometry, we introduced a Ca^{2+} source the size of which changed in response to the open fraction of IP_3R channels. This ansatz combines the deterministic spirit of the De Young Keizer model with confined Ca^{2+} liberation. The former considers a large number of IP_3R channels, which we account for by using a source density. Since the release area is bounded by some maximal radius, we satisfy the constraint of localised release. A linear stability analysis revealed that for the parameter values that De Young and Keizer originally used, oscillations do not exist. There is only one linearly stable fixed point. But even if we induce oscillations in this deterministic approach by changing some parameter values, the amplitude is too small as to be observable in experiments. Moreover, they only exist in a small window in parameter space, which renders them experimentally almost insignificant. Hence, adjusting parameter values in the original De Young Keizer model does not reinstall oscillations.

The reason why oscillations do not exist lies in the interplay between the sensitivity of gating processes and the largely elevated Ca^{2+} concentrations. A measure of those sensitivities is given by dissociation constants. Although we still lack exact numbers (see [57] in this issue for a recent contribution), we know orders of magnitude [58]. It turns out that realistic Ca^{2+} concentrations exceed these dissociation constants 10–1000 times. Taking into account that in deterministic models Ca^{2+} association and dissociation respond only to concentrations around the dissociation constants, all gating processes saturate. Hence, there is no feedback, which is essential for maintaining oscillations. Although we only considered the De Young Keizer model, these observations hold true for other gating schemes of the IP_3 receptor as well since they rely on similar dissociation constants. The only way to rescue oscillations is to resort to stochastic dynamics. The basis for fluctuations is the small number of ion channels per cluster and therefore the small number of binding sites. Since IP_3 and Ca^{2+} constantly bind and unbind at their designated binding sites, the state of an IP_3R channel changes randomly. These fluctuations are neither averaged nor even damped in a cluster due to the limited number of channels.

With these findings in our minds, we derived master equations to describe the initiation of Ca^{2+} puffs. On the one hand, we started from the master equation of a single receptor, from which we constructed channel state probabilities and then first passage time probabilities for a cluster. On the other hand, we went straight to the master equation for a channel. Although being equivalent, these two approaches differ in the distribution of computational load. The advantage of the first method lies in being exact and avoiding the combinatorial blow up present in the second way because a receptor has usually much fewer states than a channel. However, computing time scales for the first passage time probability can be easier starting from the channel master equations.

In addition to direct simulations [43, 49, 59, 60], other stochastic models have been proposed [9, 47, 61–63]. Although some of them start from a master equation, they often approximate it by a Langevin equation for computational convenience. However, such a simplification might not be applicable to an IP_3R channel cluster. These approximations rely on the presence of a large parameter as e.g. the number of ion channels or the reaction volume [38, 39], but neither of them is large in the current setting. Another step is the use of simple channel models that disregard the presence of multiple receptors. But our results indicate that the coupling between different receptors essentially shapes the probability distribution for a Ca^{2+} puff. The method that we outlined above does without any of these approximations and hence offers a powerful tool to quantify Ca^{2+} puffs.

Moving from the cluster level to whole cell dynamics, we demonstrated that stochastic Ca^{2+} puff dynamics can give rise to random whole cell Ca^{2+} oscillations. These results corroborate earlier simulations [59] and findings in Section II that the initiation of global Ca^{2+} oscillations represents indeed a nucleation process. Only the occurrence of a minimum number of nearby Ca^{2+} puffs can trigger cellular responses.

A quantitative measure of these global Ca^{2+} oscillations is the time between successive spikes, which is sometimes called the inter spike interval (ISI). The results presented here and elsewhere suggest a partition of an ISI into a stochastic and a deterministic component. The random contribution is set by the probabilities to initiate a puff and then form a critical nucleus. The deterministic time scale is controlled by spike duration and recovery from a spike. Recent experiments [48] demonstrated that the standard deviation of ISIs is similar to the average ISI. Therefore, fluctuations are of the same order as the mean, so that the stochastic time scale as quantified by waiting time distributions is not a minor aberration

of the ISI, but contributes significantly to it.

The advantage of employing waiting time densities lies in the reduction of the number of states by many orders of magnitude while conserving information on molecular fluctuations. Instead of driving stochastic multi-cluster simulations with high dimensional master equations based on single receptor dynamics, we only need to draw transition times from a probability density. The highly elevated Ca^{2+} concentrations at releasing clusters enter the calculation of waiting time densities and the coupling function, but in our approach the time evolution of these concentration fields does not depend on the simulation of a partial differential equation anymore. This results in another huge reduction in computational cost. The price that we pay for such a decrement is a Non-Markovian description [64]. Although Non-Markovian processes often escape analytical treatment, some choices of waiting time densities allow us to derive closed form expressions [64]. This is subject of ongoing research and will be presented elsewhere. In principle, the description of intracellular Ca^{2+} dynamics could become Markovian again, if we applied a quasi-steady state approximation to all transitions within the lumped states of individual clusters. However, experiments that quantify inter puff intervals clearly showed that they do not obey simple exponential distributions, indicating that the dynamics within the lumped states is relevant [65]. Information on these internal transitions is conserved in the waiting time distributions we use. These distributions can be directly measured as puff duration and inter puff interval densities, so that the formulation of our theory rests on experimentally accessible quantities.

The insights that we gain from studying intracellular Ca^{2+} dynamics extend beyond the scope of this versatile second messenger. On the one hand, localised production of signalling molecules is shared by many other cellular pathways as e.g. cAMP cascades. The growing interest in microdomains [66] and confined G-protein coupled receptor signalling [67] represent other applications. At the same time, there is a renewed interest in waiting time distributions within the physics community [64], where they arise naturally in the theory of hierarchical dynamical systems. Taken all this together, intracellular Ca^{2+} might bridge the gap between originally unrelated fields.

Parameter	Value (Set 1)	Value (Set 2)	
Geometric parameters			
height of the cytosol	9		μm
radius of the cytosol	12		μm
height of the ER h_{ER}	0.028	0.060	μm
radius of the ER R_{ER}	12		μm
leak flux coefficient P_l	0.02		μms^{-1}
Channel flux constants			
Ψ	9.3954		μms^{-1}
α	$1.497 \cdot 10^{-3}$		
β	$1.1949 \cdot 10^{-4}$		
γ	$1.1444 \cdot 10^{-7}$		μM^{-1}
δ	$1.1556 \cdot 10^{-7}$		μM^{-1}
single channel radius R_s	0.006		μm
pump flux coefficient P_p	40		$\mu\text{M}\mu\text{ms}^{-1}$
pump diss. coefficient K_d	0.2		μM
Diffusion coefficient			
D	223		$\mu\text{m}^2\text{s}^{-1}$
D_E	223	110	$\mu\text{m}^2\text{s}^{-1}$
D_m	40		$\mu\text{m}^2\text{s}^{-1}$
D_{Em}	30	16.95	$\mu\text{m}^2\text{s}^{-1}$
On-rates of buffers			
k_s^+	50		$(\mu\text{Ms})^{-1}$
k_m^+	700		$(\mu\text{Ms})^{-1}$
k_{Es}^+	1		$(\mu\text{Ms})^{-1}$
k_{Em}^+	1		$(\mu\text{Ms})^{-1}$
Buffer dissociation constants $K_i = \frac{k_i^-}{k_i^+}$			
K_s	2		μM
K_m	0.2428		μM
K_{Es}	350		μM
K_{Em}	350		μM
Total concentrations of buffers			
B_s	80		μM
B_m	40		μM
B_{Es}	50	5	mM
B_{Em}	50	5	mM
total concentration of Ca^{2+} in the ER	67.87	7.430	mM
resting concentration of free Ca^{2+} in the ER	715.56		μM

TABLE I: Parameter values for Section II. Voids in the value column of Set 2 mean that the value of Set 1 is valid.

Parameter	Value	Parameter	Value
a_0	550.0 s ⁻¹	b_0	80.0 s ⁻¹
K_1	0.0036 μM	a_1	60.0 (μMs) ⁻¹
K_2	16.0 μM	a_2	0.2 (μMs) ⁻¹
K_3	0.8 μM	a_3	5.0 (μMs) ⁻¹
K_4	0.072 μM	a_4	0.5 (μMs) ⁻¹
K_5	0.8 μM	a_5	150.0 (μMs) ⁻¹

TABLE II: Parameter values for the left panel in Figure 11. See [43, 44] for details.

Parameter	Value	Parameter	Value
k_2	37.4 (μMs) ⁻¹	k_{-2}	1.4 s ⁻¹
k_3	0.11 (μMs) ⁻¹	k_{-3}	29.8 s ⁻¹
k_4	4.0 (μMs) ⁻¹	k_{-4}	0.37 s ⁻¹
k_5	2.0 (μMs) ⁻¹	l_1	10.0 (μMs) ⁻¹
l_3	100.0 (μMs) ⁻¹	l_5	0.1 (μMs) ⁻¹
L_1	0.12 μM	L_3	0.025 μM
L_5	38.2 μM	l_2	1.7 s ⁻¹
l_{-2}	0.8 s ⁻¹	l_4	37.4 (μMs) ⁻¹
l_{-4}	2.5 s ⁻¹	l_6	4707.0 s ⁻¹
l_{-6}	11.4 s ⁻¹		

TABLE III: Parameter values for the right panel in Figure 11. See [29] for details.

-
- [1] B. Alberts, D. Bray, J. Lewis, M. Raff, K. Roberts, and J. Watson, *Molecular Biology of the Cell* (Garland Publishing, New York, 1994), 3rd ed.
 - [2] S. C. Tovey, S. G. Dedos, E. J. Taylor, J. E. Church, and C. W. Taylor, *The Journal of Cell Biology* **183**, 297 (2008).
 - [3] M. Berridge, P. Lipp, and M. Bootmann, *Nature Reviews Molecular Cell Biology* **1**, 11 (2000).
 - [4] M. J. Berridge, *Neuron* **21**, 13 (1998).
 - [5] J. Marchant and I. Parker, *The EMBO Journal* **20**, 65 (2001).
 - [6] I. Bezprozvanny, J. Watras, and B. Ehrlich, *Nature* **351**, 751 (1991).
 - [7] Taufiq-Ur-Rahman, A. Skupin, M. Falcke, and C. W. Taylor, *Nature* **458**, 655 (2009).
 - [8] S. Swillens, G. Dupont, L. Combettes, and P. Champeil, *Proceedings of the National Academy of Sciences USA* **96**, 13750 (1999).

Parameter	Value	Parameter	Value
a_1	$20 (\mu\text{Ms})^{-1}$	b_1	2.6 s^{-1}
a_2	$0.001 (\mu\text{Ms})^{-1}$	b_2	0.03077 s^{-1}
a_3	$20 (\mu\text{Ms})^{-1}$	b_3	2.6 s^{-1}
a_4	$0.025 (\mu\text{Ms})^{-1}$	b_4	0.1 s^{-1}
a_5	$10 (\mu\text{Ms})^{-1}$	b_5	12.25 s^{-1}

TABLE IV: Parameter values for the De Young Keizer model used in Figure 12. See [12] for details.

- [9] J. W. Shuai and P. Jung, *Biophysical Journal* **83**, 87 (2002).
- [10] A. Goldbeter, G. Dupont, and M. Berridge, *Proceedings of the National Academy of Sciences USA* **87**, 1461 (1990).
- [11] T. Meyer and L. Stryer, *Proceedings of the National Academy of Sciences USA* **85**, 5051 (1988).
- [12] G. De Young and J. Keizer, *Proceedings of the National Academy of Sciences* **89**, 9895 (1992).
- [13] Y. Tang, J. L. Stephenson, and H. G. Othmer, *Biophysical Journal* **70**, 246 (1996).
- [14] Y. Li and J. Rinzel, *Journal of Theoretical Biology* **166**, 461 (1994).
- [15] J. Sneyd, M. Falcke, J. F. Dufour, and C. Fox, *Progress in Biophysics and Molecular Biology* **85**, 121 (2004).
- [16] C. Taylor and J. Swatton, in *Understanding Calcium Dynamics - Experiments and Theory*, edited by M. Falcke and D. Malchow (Springer, Berlin, 2003), *Lecture Notes in Physics*, chap. 1, pp. 1–16.
- [17] R. Thul, T. C. Bellamy, H. L. Roderick, M. D. Bootman, and S. Coombes, in *Cellular Oscillatory Mechanisms*, edited by M. Maroto and N. Monk (Springer, 2008), chap. 1, pp. 1–27.
- [18] J. Keener and J. Sneyd, *Mathematical Physiology* (Springer, New York, 1998).
- [19] I. Bezprozvanny and B. Ehrlich, *The Journal of General Physiology* **104**, 821 (1994).
- [20] R. Thul and M. Falcke, *Biophysical Journal* **86**, 2660 (2004).
- [21] W. Press, S. Teukolsky, W. Vetterling, and B. Flannery, *Numerical recipes in C++* (Cambridge University Press, Cambridge, 2002), 2nd ed.
- [22] Q.-X. Jiang, E. C. Thrower, D. W. Chester, B. E. Ehrlich, and F. J. Sigworth, *The EMBO Journal* **21**, 3575 (2002).
- [23] W. Suhara, M. Kobayashi, H. Sagara, K. Hamada, T. Goto, I. Fujimoto, K. Torimitsu, and K. Mikoshiba, *Neuroscience Letters* **391**, 102 (2006).
- [24] B. Hille, *Ion Channels of Excitable Membranes* (Sinauer Associates, Sunderland, MA USA, 2001), 3rd ed.
- [25] R. Mejia-Alvarez, C. Kettlun, E. Rios, and M. Stern, *The Journal of General Physiology* **113**, 177 (1999).
- [26] D. Mak, S. McBride, and J. Foskett, *The Journal of General Physiology* **117**, 435 (2001).

- [27] D. Mak and J. Foskett, *American Journal of Physiology – Cell Physiology* **275**, C179 (1998).
- [28] A. Atri, J. Amundson, D. Clapham, and J. Sneyd, *Biophysical Journal* **65**, 1727 (1993).
- [29] J. Sneyd and J.-F. Dufour, *Proceedings of the National Academy of Sciences USA* **99**, 2398 (2002).
- [30] R. Thul, Ph.D. thesis, Freie Universität Berlin (2005).
- [31] T. R. Shannon, F. Wang, J. Puglisi, C. Weber, and D. M. Bers, *Biophysical Journal* **87**, 3351 (2004).
- [32] J. Watras, I. Bezprozvanny, and B. Ehrlich, *Journal of Neuroscience* **11**, 3239 (1991).
- [33] R. Thul and M. Falcke, *Physical Biology* **2**, 51 (2005).
- [34] J. Ramos-Franco, M. Fill, and G. Mignery, *Biochemical Journal* **75**, 834 (1998).
- [35] D. Colquhoun and A. G. Hawkes, *Philosophical Transactions of the Royal Society of London B, Biological Sciences* **300**, 1 (1982).
- [36] D. Colquhoun, A. G. Hawkes, A. Merlushkin, and B. Edmonds, *Philosophical Transactions of the Royal Society London A* **355**, 1743 (1997).
- [37] S. Redner, *A Guide to First-Passage Processes* (Cambridge University Press, 2001).
- [38] C. Gardiner, *Handbook of Stochastic Methods* (Springer, Berlin, 2004), 3rd ed.
- [39] N. van Kampen, *Stochastic Processes in Physics and Chemistry* (North-Holland, Amsterdam, 2001).
- [40] R. Thul and M. Falcke, *Europhysics Letters* **79**, 38003 (2007).
- [41] W. Feller, *An Introduction to Probability Theory and Its Applications*, vol. 1 (Wiley, New York, 1968), 3rd ed.
- [42] E. R. Higgins, H. Schmidle, and M. Falcke, *Journal of Theoretical Biology* **259**, 338 (2009).
- [43] S. Rüdiger, J. W. Shuai, W. Huisinga, C. Nagaiah, G. Warnecke, I. Parker, and M. Falcke, *Biophysical Journal* **93**, 1847 (2007).
- [44] J. Shuai, J. E. Pearson, J. K. Foskett, D.-O. D. Mak, and I. Parker, *Biophysical Journal* **93**, 1151 (2007).
- [45] C. Adkins and C. Taylor, *Current Biology* **9**, 1115 (1999).
- [46] M. Falcke, *Advances in Physics* **53**, 255 (2004).
- [47] G. Ullah and P. Jung, *Biophysical Journal* **90**, 3485 (2006).
- [48] A. Skupin, H. Kettenmann, U. Winkler, M. Wartenberg, H. Sauer, S. C. Tovey, C. W. Taylor, and M. Falcke, *Biophysical Journal* **94**, 2404 (2008).
- [49] G. Dupont, A. Abou-Lovergne, and L. Combettes, *Biophysical Journal* **95**, 2193 (2008).
- [50] I. F. Smith, S. M. Wiltgen, and I. Parker, *Cell Calcium* **45**, 65 (2009).
- [51] K. Bentele and M. Falcke, *Biophysical Journal* **93**, 2597 (2007).
- [52] J. K. Foskett, C. White, K.-H. Cheung, and D.-O. D. Mak, *Physiological Reviews* **87**, 593 (2007).
- [53] G. Barton, *Elements of Green's Functions and Propagation* (Oxford University Press, Oxford, 1989).

- [54] A. Alfonsi, E. Cancès, G. Turinici, B. D. Ventura, and W. Huisinga, Tech. Rep. 5434, INRIA (2004).
- [55] S. Patel, S. K. Joseph, and A. P. Thomas, *Cell Calcium* **25**, 247 (1999).
- [56] B. Devogelaere, L. Verbert, J. B. Parys, L. Missiaen, and H. De Smedt, *Cell Calcium* **43**, 17 (2008).
- [57] E. Gin and J. Sneyd, *Chaos* (2009).
- [58] R. Thul and M. Falcke, *Physical Review Letters* **93**, 188103 (2004).
- [59] M. Falcke, *Biophysical Journal* **84**, 42 (2003).
- [60] G. Solovey, D. Fraiman, B. Pando, and S. P. Dawson, *Physical Review E* **78**, 041915 (pages 15) (2008).
- [61] J. W. Shuai and P. Jung, *Physical Review Letters* **88**, 068102 (2002).
- [62] V. Nguyen, R. Mathias, and G. D. Smith, *Bull. Math. Biol.* **67**, 393 (2005).
- [63] H. DeRemigio and G. D. Smith, *Cell Calcium* **38**, 73 (2005).
- [64] T. Prager, M. Falcke, L. Schimansky-Geier, and M. A. Zaks, *Physical Review E* **76**, 011118 (pages 13) (2007).
- [65] I. F. Smith and I. Parker, *Proceedings of the National Academy of Sciences* **106**, 6404 (2009).
- [66] M. J. Berridge, *Cell Calcium* **40**, 405 (2006).
- [67] S. J. Hill, *British Journal of Pharmacology* **147**, S27 (2006).